Changes in Moisture Flux over the Tibetan Plateau during 1979–2011 and Possible Mechanisms

YANHONG GAO

Key Laboratory of Land Surface Process and Climate Change in Cold and Arid Regions, Cold and Arid Regions Environmental and Engineering Research Institute, Chinese Academy of Sciences, Lanzhou, China

LAN CUO

Key Laboratory of Tibetan Environmental Changes and Land Surface Processes, Institute of Tibetan Plateau Research, Chinese Academy of Sciences, Beijing, China

YONGXIN ZHANG

Research Applications Laboratory, National Center for Atmospheric Research, Boulder, Colorado

(Manuscript received 13 June 2013, in final form 2 November 2013)

ABSTRACT

Changes in moisture as represented by $P - E$ (precipitation − evapotranspiration) and the possible causes over the Tibetan Plateau (TP) during 1979–2011 are examined based on the Global Land Data Assimilation Systems (GLDAS) ensemble mean runoff and reanalyses. It is found that the TP is getting wetter as a whole but with large spatial variations. The climatologically humid southeastern TP is getting drier while the vast arid and semiarid northwestern TP is getting wetter. The Clausius–Clapeyron relation cannot be used to explain the changes in $P - E$ over the TP.

Through decomposing the changes in $P - E$ into three major components—dynamic, thermodynamic, and transient eddy components—it is noted that the dynamic component plays a key role in the changes of $P - E$ over the TP. The thermodynamic component contributes positively over the southern and central TP whereas the transient eddy component tends to reinforce (offset) the dynamic component over the southern and parts of the northern TP (central TP).

Seasonally, the dynamic component contributes substantially to changes in $P - E$ during the wet season, with small contributions from the thermodynamic and transient eddy components. Further analyses reveal the poleward shift of the East Asian westerly jet stream by 0.7° and poleward moisture transport as well as the intensification of the summer monsoon circulation due to global warming, which are shown to be responsible for the general wetting trend over the TP. It is further demonstrated that changes in local circulations that occur due to the differential heating of the TP and its surroundings are responsible for the spatially varying changes in moisture over the TP.

1. Introduction

Moisture is one of the most critical components of the hydrological cycle, and changes in moisture reflect shifts in the controlling atmospheric circulations and (or) underlying surface, with profound implications for weather and climate. As climate change is taking place as a result of the emissions of greenhouse gases and aerosols (Solomon et al. 2007), one important question to ask is to what degree climate change will affect moisture changes or, in other words, how moisture will respond to climate change. Important insights have been gained into the responses of moisture to climate change both globally and over several parts of the world including the tropics, North America, and Europe (e.g., Held and Soden 2006; Kassomenos and McGregor 2006; Lorenz and DeWeaver 2007; Chou et al. 2009; Gao et al. 2012; Chou and Lan 2012; Seager and Naik 2012; Chou et al. 2013). Over the Tibetan Plateau (TP; Fig. 1), however, such topics as how moisture changes in response to climate change and what

Corresponding author address: Dr. Yanhong Gao, 320 Donggang West Rd., Cold and Arid Regions Environmental and Engineering Research Institute, Chinese Academy of Sciences, Lanzhou 730000, China.
E-mail: gaoyh@lzb.ac.cn

DOI: 10.1175/JCLI-D-13-00321.1

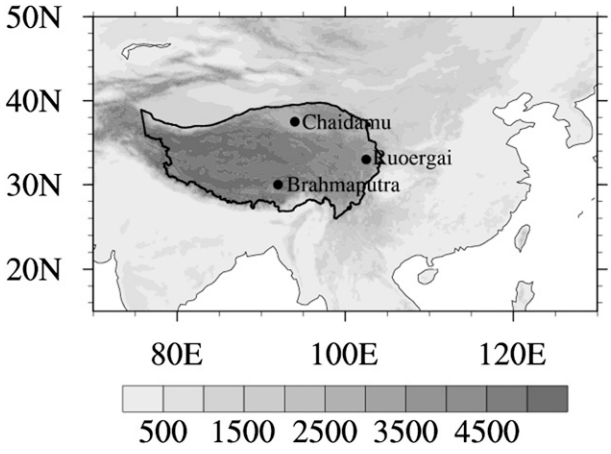

FIG. 1. Geographic location and the elevation (m) of the Tibetan Plateau.

are the mechanisms behind the moisture changes have not been fully explored despite the fact that the TP exerts significant influence on regional and global climate and that it provides a main passage for water vapor and chemicals to reach the stratosphere (Fu et al. 2006).

During the past three decades, the TP has been experiencing climate change (Pan and Li 1996; Kang et al. 2010), with the warming rate over the TP much larger than that of the global average or of the same latitudes in the Northern Hemisphere during the same time period (Liu and Chen 2000; Wu et al. 2007; Solomon et al. 2007; Krause et al. 2010; Moore 2012). While the warming over the TP reflects the anthropogenic warming signal worldwide, its high terrain, extensive size, and particular location likely contribute to the accelerated warming rate. Unlike temperature, precipitation and snow over the TP do not show consistent and plateau-wide changes during the past decades; however, a majority of the gauge records and station measurements have exhibited increasing trends in precipitation, lake area, and water level (Bian et al. 2006; You et al. 2008; Wu and Zhu 2008; Zhu et al. 2010; Yao et al. 2012). A few other studies also report positive $P - E$ (i.e., precipitation minus evapotranspiration) changes over the TP (Shi et al. 2007; Krause et al. 2010; Yang et al. 2011; Yin et al. 2012), indicating that the TP is getting wetter in general. Where the extra moisture come from and what mechanisms are responsible for the moisture changes over the TP are, however, unclear and certainly merit further investigation.

More than 99% of the total moisture in the atmosphere is in the form of water vapor. Lower-tropospheric water vapor increases as the climate warms as dictated by the Clausius–Clapeyron (C-C) relation under the condition that the relative humidity in the lower troposphere stays constant (Held and Soden 2006; Wentz et al. 2007). The C-C relation also assumes that the water cycle will intensify as climate becomes warmer. The climate change experiments generated for the Fourth Assessment Report (AR4) of the Intergovernmental Panel on Climate Change (IPCC) predict that changes in $P - E$ will vary proportionally to the lower-tropospheric water vapor (Held and Soden 2006), indicating that the wet becomes wetter and the dry becomes drier (Seager and Vecchi 2010; Seager et al. 2010). According to the above theory, the climatologically arid and semiarid northern and northwestern TP with annual precipitation less than 200 mm should become drier while the southeastern TP with annual precipitation larger than 600 mm (Yao et al. 2012) should become wetter. However, precipitation and discharge gauge records show a different pattern, with generally wetting trends over the northwestern TP and drying trends over the southeastern TP (Yang et al. 2011; Yin et al. 2012). Zhang et al. (2012) and Gao et al. (2012) report enhanced poleward moisture transport and amplified wetting trends in the northern high latitudes. Could this poleward moisture transport be used to explain the wetting trends over the northwestern TP? What is then behind the drying trends over the southeastern TP? Answers to these questions could potentially reveal the mechanisms of moisture transport and redistribution, as well as hydrological cycle changes in response to rapid warming over the TP.

The objectives of the current study are twofold: 1) to identify the hydrological cycle change over the TP during the recent decades, and 2) to explore the mechanisms of the hydrological cycle change. The rest of the paper is organized as follows. Section 2 introduces the methodology and the datasets used. Section 3 examines the climatology of moisture and changes in the hydrological cycle as represented by $P - E$. Section 4 investigates the possible mechanisms of the hydrological cycle change. Major conclusions and discussions are presented in section 5.

2. Data and methodology

a. $P - E$ data

In the terrestrial hydrological cycle, $P - E$ is equivalent to the long-term averaged runoff or water resources over the land. $P - E$ over the land comes almost entirely from three sources: evaporation from any moist surface or body of water, evaporation from soil, and transpiration from plants. Although oceans are the most important moisture source globally because they occupy three-quarters of Earth's surface, land sources can be important locally. Because of the scarcity and quality issues of

the observed runoff and evapotranspiration, most $P - E$ analyses rely on land surface model simulated runoff and evapotranspiration (Yang et al. 2011; Yin et al. 2012). Such simulations are assumed to reasonably well represent the real situations since the model forcing data such as precipitation, temperature, and radiation are observed and the models are physically based and are subject to vigorous evaluation. One notable example is the Global Land Data Assimilation Systems (GLDAS) (Rodell et al. 2004), which incorporate observation-based atmospheric data, remote sensing data, and reanalysis as forcing fields to drive multiple land surface models [e.g., Noah, the Community Land Model (CLM), Variable Infiltration Capacity (VIC), and Mosaic] and produce optimal fields of land surface states and fluxes starting from 1979. The sources of data that have been used in GLDAS are briefly described in the following.

Downward shortwave and longwave radiation fluxes at the land surface were estimated using algorithms of Shapiro (1987) and Idso (1981) and cloud and snow products from the Air Force Weather Agency's (AFWA) Agricultural Meteorology modeling system (AGRMET). The cloud and snow products were derived primarily from observations made by Defense Meteorological Satellite Program and National Oceanic and Atmospheric Administration (NOAA) satellites. Near-real-time satellite-derived precipitation data were obtained from the U.S. Naval Research Laboratory (NRL) and Goddard Space Flight Center (GSFC). NRL's precipitation fields were based on geostationary satellite infrared (IR) cloud-top temperature measurements and microwave observation techniques (Turk et al. 2000). The microwave product merged data from the Special Sensor Microwave/Imager (SSM/I), the National Aeronautics and Space Administration (NASA)–Japan Aerospace Exploration Agency (JAXA) Tropical Rainfall Measuring Mission (TRMM), and the Advanced Microwave Sounding Unit (AMSU) instruments. GSFC's precipitation fields were based on the optimal merging of microwave measurements from the Advanced Microwave Scanning Radiometer (AMSR) and the *Advanced Earth Observation Satellite* II (ADEOS-II) besides SSM/I and TRMM with the more frequent IR measurements from the international constellation of geosynchronous-Earth-orbit (GEO) satellites (Huffman et al. 2003). For boundary and initial conditions, GLDAS made use of the analyses from the Global Data Assimilation System (GDAS; Derber et al. 1991) that assimilated a variety of conventional data (radiosonde, buoy, ship, and airborne) and satellite-derived observations using a four-dimensional multivariate approach (Rodell et al. 2004).

Over the TP, Wang and Zeng (2012) showed that among the most widely used reanalysis products, GLDAS exhibits the best overall performance in both daily and monthly precipitation as well as satisfactory performance for other surface variables. Therefore, the GLDAS data are used in this study as the ''ground truth'' although it is recognized that the GLDAS data also contain uncertainties. It is worth mentioning that examining surface runoff alone only reveals $P - E$ change from the perspective of land surface processes, whereas analysis of $P - E$ change over the land and the causes of the change can help to identify changes in the atmospheric hydrological cycle.

b. Reanalyses

Vertically integrated moisture flux convergence is equivalent to the long-term mean of $P - E$ or runoff (Trenberth and Guillemot 1995; Seager and Vecchi 2010; Seager et al. 2007, 2010; Gao et al. 2012). In this study, $P - E$ represented by the vertically integrated moisture flux convergence in 1979–2011 is calculated using four reanalysis datasets. These four datasets are the National Centers for Environmental Prediction (NCEP)–National Center for Atmospheric Research (NCAR) reanalysis (1948–present; Kalnay et al. 1996), the NCEP–Department of Energy (DOE) reanalysis (1979–present; Kanamitsu et al. 2002), the 40-yr European Centre for Medium-Range Weather Forecasts (ECMWF) Re-Analysis (ERA-40; 1958–2002; Uppala et al. 2005), and the Interim ECMWF Re-Analysis (ERA-Interim, also called ERA-Int herein; 1979–present; Simmons et al. 2006). All of these reanalyses utilize conventional data sources such as radiosonde, buoy, and ship data, while other sources such as precipitation and satellites are utilized differently depending on the reanalysis. Over the TP, with scarce observations and complex terrain, each reanalysis may contain varying degrees of deficiencies. By using four datasets, our hope is to find the optimal reanalysis for use in the examination of the moisture changes over the TP. A brief summary of these reanalyses follows.

1) NCEP–NCAR

The NCEP–NCAR reanalysis uses the NCEP global atmospheric spectral model with 28 vertical levels and a horizontal resolution of approximately 210 km (Kalnay et al. 1996). The land surface model is the Oregon State University land surface model with two vertical layers. The assimilation of observations is achieved through the use of a three-dimensional variational data assimilation (3DVar) approach. The assimilated observations include radiosondes, satellite retrievals of atmospheric temperature, satellite-based winds from cloud tracking, aircraft observations of temperature and wind, and land and oceanic surface pressure measurements.

2) NCEP–DOE

The NCEP–DOE reanalysis is the updated version of the NCEP–NCAR reanalysis: both reanalyses are run with the same spatial resolution and use similar observational data (Kanamitsu et al. 2002). Major differences between the two reanalyses include the following: 1) the starting year is 1979 for NCEP–DOE whereas it is 1948 for NCEP–NCAR; 2) simple rainfall assimilation over land surfaces is used for NCEP–DOE but not for NCEP–NCAR; 3) model physics (such as planetary boundary layer, radiation, and convective parameterization) and fixed fields (such as albedo, SST, and snow cover) improvements since the release of the NCEP–NCAR reanalysis have been utilized for NCEP–DOE; and 4) known errors in NCEP–NCAR have been fixed in NCEP–DOE.

3) ERA-40

The ERA-40 reanalysis uses the ECMWF forecasting model version cycle 23r4, with 60 vertical levels at a horizontal resolution of around 125 km (Uppala et al. 2005). The data assimilation system is based on the 3DVar approach with an analysis cycle of 6 h. ERA-40 incorporates types of observational data that are very similar to NCEP–NCAR and NCEP–DOE but with one significant exception: ERA-40 includes observed 2-m air temperature and relative humidity from weather stations for adjusting surface temperature and soil moisture.

4) ERA-INT

The ERA-Interim reanalysis is an improved version of the ERA-40 reanalysis (Simmons et al. 2006). An updated ECMWF forecasting model version cycle 31r1 is used with a horizontal resolution of approximately 80 km for ERA-Int. Aside from the improved resolution over ERA-40, ERA-Int utilizes four-dimensional variational data assimilation (4DVar) and variational bias correction of satellite radiance data (Dee and Uppala 2009), better formulation of background error constraint, new humidity analysis, and improved model physics. ERA-Int also uses mostly the sets of observations acquired for ERA-40, supplemented by data for later years from ECMWF's operational archive. In addition, ERA-Int makes extensive use of radiances such as altimeter wave heights and radio occultation measurements. As with ERA-40, the land surface analysis for ERA-Int incorporates 2-m air temperature and relative humidity to improve the land surface model temperature and soil moisture fields.

c. Methodology

To calculate the vertically integrated moisture flux convergence, 6-hourly specific humidity and wind data at standard pressure levels in 1979–2011 (1979–2002 for ERA-40) are used. The spatial derivatives are discretized with centered second-order differences dropping to one-sided first-order differences at points adjacent to undefined values (Seager et al. 2007). The vertical integral is performed at the standard pressure levels assuming a piecewise linear profile from the surface to the top level of the datasets that can be integrated exactly to give a second-order approximation (Gao et al. 2012).

The moisture budget equation could be written as

$$\rho_w g(\overline{P} - \overline{E}) = -\int_0^{p_s} \nabla \cdot (\overline{\mathbf{V}}\,\overline{q})\, dp - \int_0^{p_s} \nabla \cdot (\overline{\mathbf{V}'q'})\, dp - \overline{q_s \mathbf{V}_s \cdot \nabla p_s}, \quad (1)$$

where overbars represent the means, primes denote departures from the means, ρ_w is the density of water, g is the acceleration due to gravity, subscript s represents surface, and ∇ indicates the horizontal divergence operator. Atmospheric flow and moisture are denoted by $\mathbf{V}$ and q, respectively. On the right-hand side of (1), the first integral describes moisture convergence by the mean flow, the second term is the convergence by transient eddies (Trenberth and Guillemot 1995), and the third term represents surface contributions, which normally have maximum values a few times smaller than the other terms (Seager et al. 2007).

In this study, the ensemble mean of runoff from GLDAS is used to compare with $P - E$ values obtained from the four reanalyses. Temporal and spatial correlation coefficients between the reanalyses and the GLDAS ensemble mean are calculated for evaluating the performance of each reanalysis in representing the climatology and trends of $P - E$. To calculate the spatial correlation coefficients, $P - E$ estimates from NCEP–NCAR, NCEP–DOE, ERA-40, and GLDAS were interpolated to the common ERA-Int grid at 0.7° resolution.

To account for the moisture change over the TP, we follow the approach by Seager and Vecchi (2010) and Seager et al. (2010), who examined the causes of global hydrological change by decomposing Eq. (1) into different components representing different contributors. This approach was also used to analyze the causes of megadrought over the Colorado River basin in the southwestern United States (Gao et al. 2012).

Guo et al. (2011) reported that river discharge changed dramatically after 1998 in the Heihe River basin located in the northern TP during 1957–2008. Observed annual surface air temperature and precipitation averaged across the TP also showed abrupt changes around 1998 (Fig. 2). The time series of the GLDAS ensemble mean runoff

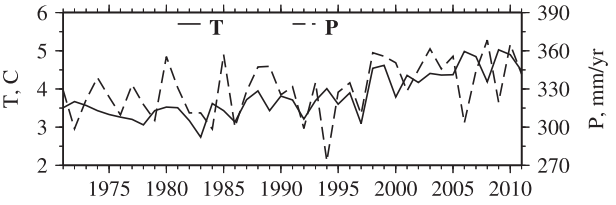

FIG. 2. Observed annual mean surface air temperature (T, °C) and precipitation (P, mm yr^{-1}) in 1971–2011 averaged over the TP. The observations came from 83 ground stations over the TP, and were first interpolated into a 1° × 1° grid and then averaged over the TP.

averaged over the TP (not shown) revealed a similar pattern in 1979–97 and 1998–2011 to that reported in Guo et al. (2011) for the same time periods. In the following analysis, 1998 is treated as a pivotal year, and changes in moisture before and after the pivotal year, which are regarded as the moisture trend over the TP in 1979–2011, are explored.

Denoting

$$\delta(\cdot) = (\cdot)_{\text{post}} - (\cdot)_{\text{pre}}, \tag{2}$$

where subscripts pre and post represent prephase (1979–1997) and postphase (1998–2011), respectively. The changes of $P - E$ in postphase relative to prephase are decomposed to mean moisture flux convergence and transient eddy moisture convergence (TE):

$$\rho_w g\delta(\overline{P} - \overline{E}) = -\int_0^{p_s} \nabla \cdot \delta(\overline{\mathbf{V}}\,\overline{q})\,dp - \int_0^{p_s} \nabla \cdot \delta(\overline{\mathbf{V}'q'})\,dp - \delta S, \tag{3}$$

where $\delta S = \delta(\overline{q_s \mathbf{V}_s \cdot \nabla p_s})$ represents the changes in surface contributions. Since surface contributions normally have maximum values a few times smaller than the other terms in Eq. (1) (not shown; see also Seager et al. 2007), their changes are small and negligible. This is also confirmed by examining the sum of the changes in the other terms (not shown).

Mean moisture flux convergence change is further separated into a thermodynamic contributor (TH) due to changes in mean specific humidity ($\overline{q}$) and dynamic contributor due to changes in mean circulation ($\overline{\mathbf{V}}$). Since transient eddy moisture convergence cannot be divided into eddy humidity and eddy flow components in a straightforward way, it remains unchanged following Seager et al. (2010). Seager et al. (2010) also found that the changes in the product of mean eddy specific humidity and eddy flow circulation ($\overline{V'q'}$) were small and could be neglected. Consequently, the $P - E$ changes are treated as a combination of thermodynamic, mean circulation dynamics (MCD), and transient eddy components as denoted in the following:

$$\rho_w g\delta(\overline{P} - \overline{E}) \approx \delta\text{TH} + \delta\text{MCD} + \delta\text{TE} - \delta S,$$

$$\delta\text{TH} = -\int_0^{p_s} \nabla \cdot (\overline{\mathbf{V}}_{\text{pre}}[\delta\overline{q}])\,dp,$$

$$\delta\text{MCD} = -\int_0^{p_s} \nabla \cdot ([\delta\overline{\mathbf{V}}]\overline{q}_{\text{pre}})\,dp, \quad \text{and}$$

$$\delta\text{TE} = -\int_0^{p_s} \nabla \cdot \delta(\overline{\mathbf{V}'q'})\,dp. \tag{4}$$

3. Results and discussion

a. Climatology and changes of $P - E$ over the TP during 1979–2011

On annual average, the vertically integrated moisture fluxes over the TP based on ERA-Int are dominated by the westerly component in the zonal direction (Fig. 3a). This is clearly due to the westerly winds that affect the TP year around (e.g., Tian et al. 2007; Schiemann et al. 2008; Duan and Wu, 2008, 2009). Meridionally, negative (positive) moisture fluxes are identified to the north (south) of 34°–35°N over the TP (Fig. 3b), due to the southward (northward) moving cold and dry high- to midlatitude air (warm and wet subtropical air), as will be shown later. It appears that 34°–35°N is the northern boundary of the South Asian monsoon (Tian et al. 2007; Conroy and Overpeck 2011). Similar distributions in the vertically integrated moisture fluxes are also noted for the other three reanalyses (not shown).

The GLDAS ensemble mean runoff over the TP generally decreases from the southeast to the northwest (Fig. 4a), largely consistent with the annual mean precipitation patterns (Ge et al. 2008; Cuo et al. 2013). The plateau-wise mean runoff from GLDAS is 0.28 mm day^{-1} (Table 1), which is comparable to 0.24 mm day^{-1} reported by Yin et al. (2012), who examined the impact of climate change on actual evapotranspiration over the TP during 1981–2010. Yin et al. (2012) also showed a decreasing pattern of runoff from the southeast to the northwest, with higher $P - E$ (~0.66 mm day^{-1}) in the humid southeastern TP and lower $P - E$ (~0.05 mm day^{-1}) in the arid northwestern TP.

In comparison, $P - E$ estimates over the TP by four reanalyses (Figs. 4b–e) show varying degrees of success in resolving the GLDAS ensemble mean runoff. All four reanalyses represent high $P - E$ over the southeastern TP, while over the northwestern TP only ERA-Int corresponds to low $P - E$ as in the GLDAS ensemble mean

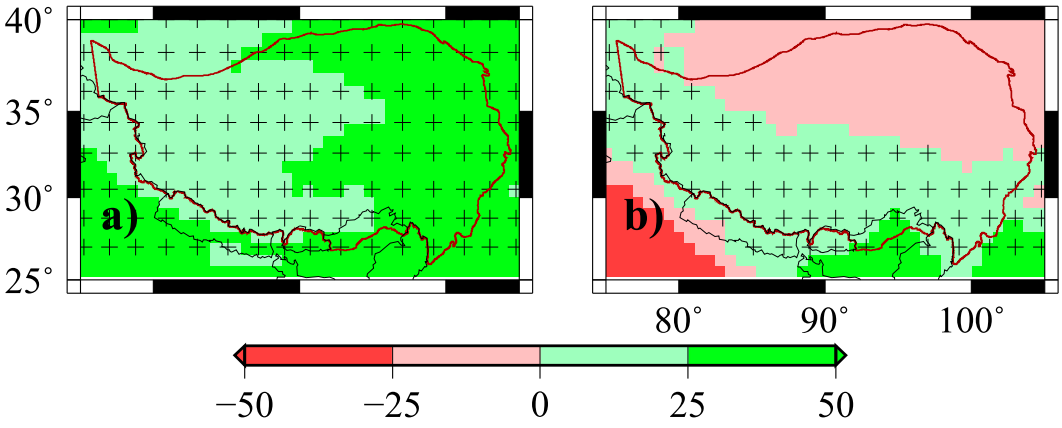

FIG. 3. Climatology of the vertically integrated (a) mean zonal and (b) mean meridional moisture fluxes ($kg\,m^{-1}\,s^{-1}$) over the Tibetan Plateau for 1979–2011 constructed from the ERA-Interim (ERA-Int) reanalysis. Positive to east for zonal fluxes and to north for meridional fluxes. Positive values hereafter are also marked by crosses.

runoff. Averaged across the TP, all four reanalyses generate much larger $P - E$ than the GLDAS ensemble mean runoff ($0.28\,mm\,day^{-1}$): $1.28\,mm\,day^{-1}$ for NCEP–NCAR, $1.16\,mm\,day^{-1}$ for NCEP–DOE, $1.22\,mm\,day^{-1}$ for ERA-40, and $0.92\,mm\,day^{-1}$ for ERA-Int (Table 1). The reason for the overestimation of $P - E$ by the reanalyses is due to the overestimation of precipitation: all four reanalyses generate approximately twice as much precipitation as the GLDAS ensemble mean precipitation while the evapotranspiration for the reanalyses is comparable to that of the GLDAS ensemble mean (not shown).

Spatial correlations between $P - E$ estimates by the reanalyses and the GLDAS ensemble mean runoff are relatively high at 0.49, 0.44, 0.62, and 0.71 for NCEP–NCAR, NCEP–DOE, ERA-40, and ERA-Int, respectively, and are all statistically significant at the 99.9% confidence level with a degree of freedom of 518 (i.e., the number of ERA-Int grid points minus 1) (Table 1). What is evident is that among the four reanalyses ERA-Int resolves the GLDAS ensemble mean runoff the best as reflected by the southeast–northwest moisture gradient, the closest domain averages, and the highest correlation.

The GLDAS ensemble mean annual runoff exhibits a positive trend of $0.004\,mm\,day^{-1}$ when averaged over the TP (Table 2), consistent with Yang et al. (2011) and Yin et al. (2012). Except for NCEP–NCAR for which the estimated $P - E$ shows a negative trend of $-0.012\,mm\,day^{-1}$, the other three reanalyses all show positive trends in $P - E$ (Table 2). The ERA-40 estimated trend in $P - E$ is approximately 2 times larger than that of NCEP–DOE, ERA-Int, and the GLDAS ensemble mean runoff. Temporal correlation between the reanalyses-estimated $P - E$ and the GLDAS ensemble mean runoff varies widely among the reanalyses, with ERA-Int showing the highest correlation of 0.29 (Table 2) that is significant at the 90% confidence level but not at the 99% and 99.9% levels.

Spatially, the GLDAS ensemble mean runoff displays predominantly positive trends over the vast west TP, with negative trends over the Chaidamu basin in the northeastern part of the TP and over regions of the southern TP extending from the lower reaches of the Upper Brahmaputra River basin to the Ruoergai Plateau in the eastern TP (Fig. 5a; see Fig. 1 for the locations of Brahmaputra and Ruoergai). Yang et al. (2011) and Yin et al. (2012) also arrived at a similar spatial pattern in runoff trend. Among the four reanalyses (Figs. 5b–e), only ERA-Int resolves the predominantly positive trends over the vast west TP and the negative trends over the Chaidamu basin (Fig. 5e). Over southern TP none of the reanalyses matches the pattern of the GLDAS runoff. The spatial correlation of trends between the GLDAS ensemble mean runoff and reanalyses-estimated $P - E$ (Table 2) is very small, being positive for NCEP–NCAR and ERA-Int and negative for NCEP–DOE and ERA-40.

Both the climatology and the trend analyses indicate that ERA-Int, though far from being perfect, shows the best $P - E$ estimation among the four reanalyses over the TP. Besides being the highest-resolution reanalysis and incorporating advanced model physics, the better performance of ERA-Int is also likely due to the improvements in the hydrological cycle with its 12-h 4DVar that has a smaller model spinup/spindown issue than 3DVar (Dee et al. 2011). Previous studies also demonstrated that ERA-Int outperforms several other widely available reanalysis products in estimating climatology and variations of surface variables over the TP

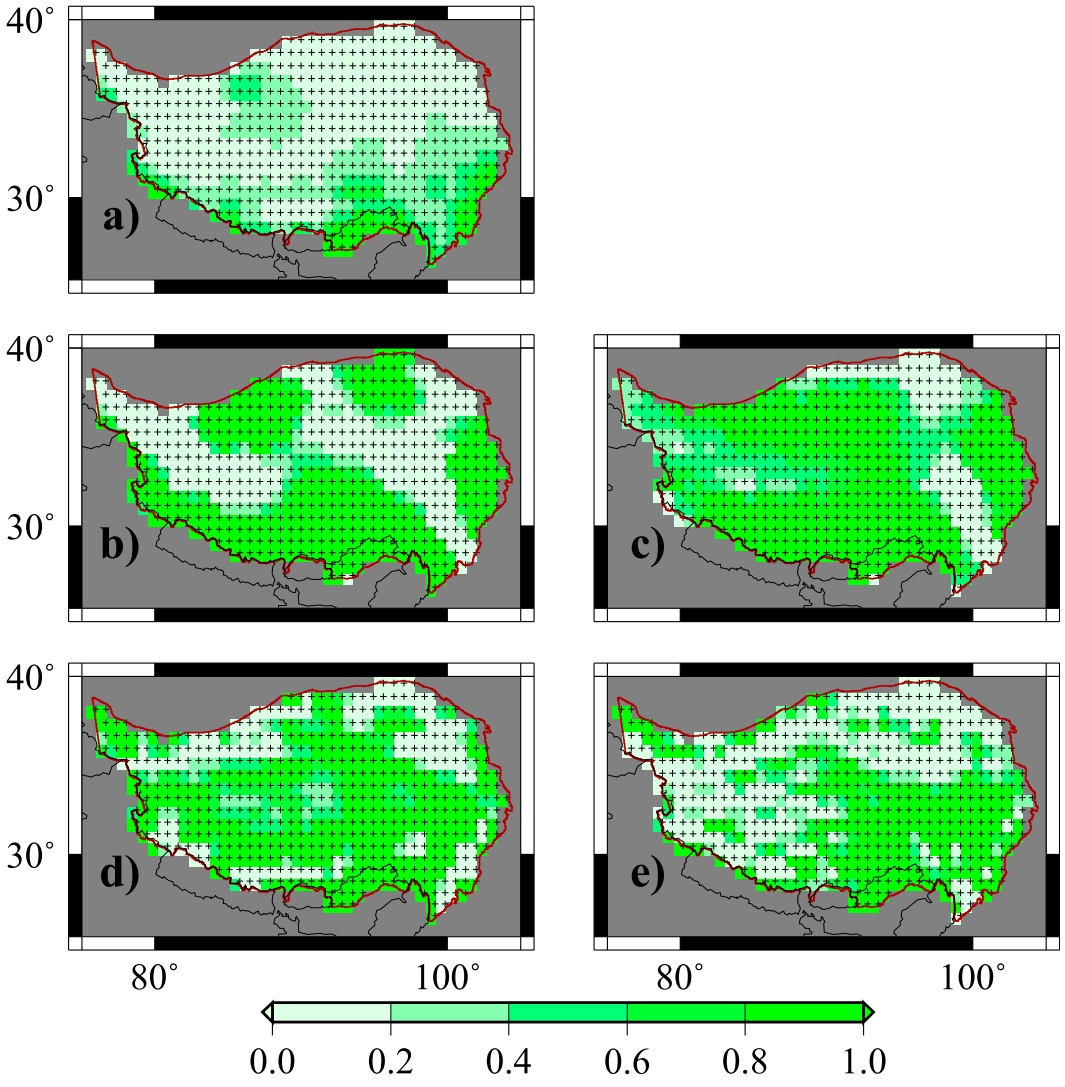

FIG. 4. Climatology of (a) runoff (mm day^{-1}) from GLDAS ensemble mean and (b)–(e) $P - E$ estimates (mm day^{-1}) from four reanalyses [(b) NCEP–NCAR, (c) NCEP–DOE, (d) ERA-40, and (e) ERA-Int] over the TP for 1979–2011.

(Wang and Zeng 2012; Li et al. 2012; Bao and Zhang 2013). Hereafter, we use ERA-Int to explore the mechanisms of the moisture trend over the TP.

b. Causes of moisture trend over the TP

1) COMPONENTS OF $P - E$ CHANGES OVER THE TP

Spatial correlation between total changes in $P - E$ and the mean circulation dynamics component, thermodynamic component, and transient eddy component in postphase relative to prephase exhibits a statistically significant correlation coefficient of 0.88 for MCD, rather small correlation coefficient of −0.12 for TH, and −0.03 for TE (Table 3). Horizontal distributions depicted in Fig. 6 show that except for the northern and northwestern parts of the TP, MCD nearly mimics the total changes in $P - E$ across the TP (Figs. 6a,b), indicating that MCD is the dominant contributor to the $P - E$ changes. TH (Fig. 6c) contributes positively in the southeastern TP where water vapor is abundant; and it contributes negatively over the vast arid and semiarid region in the northern and northwestern TP where there is not much water vapor to begin with. This is apparently in line with what the C-C relation predicts in that the wet becomes wetter and the dry become drier; however, as mentioned before, precipitation records as well as the GLDAS runoff show generally wetting trends over the northwestern TP and drying trends over the southeastern TP (Yang et al. 2011; Yin et al. 2012; Fig. 5a), which

TABLE 1. Runoff and $P - E$ means (mean, mm day^{-1}) in 1979–2011 (1979–2002 for ERA-40) averaged over the Tibetan Plateau for GLDAS (four land surface models and their ensemble means) and four reanalyses, and spatial correlation coefficients of $P - E$ means between GLDAS and reanalyses (Corr). Statistically significant values at 99.9% confidence level based on the two-paired t test are denoted in bold. The degrees of freedom for spatial correlation is 518.

Model	Mean	Corr
Noah	0.37	—
CLM	0.34	—
VIC	0.21	—
MOSAIC	0.14	—
GLDAS ensemble mean	0.28	—
NCEP–NCAR	1.28	**0.49**
NCEP–DOE	1.16	**0.44**
ERA-40	1.22	**0.62**
ERA-Int	0.92	**0.71**

TABLE 2. Runoff trends in 1979–2011 averaged over the Tibetan Plateau for GLDAS (four land surface models and their ensemble mean), $P - E$, mean zonal and meridional moisture flux (UQ, VQ) trends for four reanalyses ($P - E$, units: mm day^{-1} yr^{-1}; UQ and VQ, units: kg m^{-1} s^{-1} yr^{-1}), temporal correlation coefficients of $P - E$ averaged over the TP (Corr1) and spatial correlation coefficients of $P - E$ trends in 1979–2011 (Corr2) between the GLDAS ensemble mean and reanalyses estimates. Statistically significant values at 99.9% confidence level based on a two-paired t test are denoted in bold. The degree of freedom is 518 for spatial correlation and 32 for temporal correlation.

Model	$R/(P - E)$	UQ	VQ	Corr1	Corr2
Noah	−0.00005	—	—	—	—
CLM	0.004	—	—	—	—
VIC	0.009	—	—	—	—
MOSAIC	0.006	—	—	—	—
GLDAS ensemble mean	**0.004**	—	—	—	—
NCEP–NCAR	**−0.012**	**−0.08**	**−0.064**	−0.23	0.08
NCEP–DOE	**0.006**	**−0.12**	**0.003**	0.008	−0.01
ERA-40	**0.013**	**−0.17**	**0.006**	0.25	−0.09
ERA-Int	**0.007**	**−0.03**	**0.033**	0.29	0.04

indicates that the C-C relation cannot explain the hydrological cycle change over the TP.

TE (Fig. 6d) shows negative changes over the central TP where the terrain is relatively flat and positive changes along the southern TP and part of the northern TP where sharp gradients in terrain exist, which may imply that eddy activities tend to intensify over the complex terrain along the boundaries of the TP. You et al. (2008) noted that extreme events increase in the southern and northern TP but decrease in the central TP during 1961–2005, which could be related to changes in eddy activities associated with shifts in the large-scale circulations and local systems (e.g., Cuo et al. 2013). Comparing Fig. 6 with Fig. 5, it becomes clear that over the southeastern TP, the small but positive trends in moisture in ERA-Int are due mainly to the positive contributions from the dynamic component. In other words, the $P - E$ overestimation by ERA-Int over the southeastern TP is due to the overestimated contributions from changes in mean circulation.

Following Seager et al. (2007), we also computed the C-C approximation to the thermodynamically and transient eddy induced changes in $P - E$ ($\delta\mathrm{TH}_{\mathrm{cc}}$ and $\delta\mathrm{TE}_{\mathrm{cc}}$) as follows:

$$\delta(\overline{P} - \overline{E})_{\mathrm{cc}} = -\alpha\delta T \int_0^{p_s} \nabla \cdot (\overline{\mathbf{V}_{\mathrm{pre}} q_{\mathrm{pre}}})\, dp, \qquad (5)$$

$$\delta\mathrm{TH}_{\mathrm{cc}} = -\alpha\delta T \int_0^{p_s} \nabla \cdot (\overline{\mathbf{V}}_{\mathrm{pre}} \overline{q}_{\mathrm{pre}})\, dp, \qquad (6)$$

$$\delta\mathrm{TE}_{\mathrm{cc}} = -\alpha\delta T \int_0^{p_s} \nabla \cdot (\overline{\mathbf{V}'q'})_{\mathrm{pre}}\, dp, \qquad (7)$$

where δT refers to changes in temperature between the surface and 500 mb (1 mb = 1 hPa) and $\alpha = \delta \ln(e_s)/\delta T$, with e_s being the saturation vapor pressure. All three terms are computed independently and the sum of (6) and (7) is not equal to what (5) generates but the differences are very small.

The C-C estimated thermodynamically induced $P - E$ changes (δTHcc; Fig. 7b) exhibit a similar pattern to that by δTH (Fig. 6c) but with smaller magnitude: increases in the southeastern TP and decreases in the northern TP. Transient eddy induced $P - E$ changes (δTEcc, Fig. 7c) show a different pattern than that by δTE (Fig. 6d) in that the negative (positive) changes are located mainly over the western (eastern) TP. In comparison, the C-C estimated total changes in $P - E$ (Fig. 7a) are smaller in magnitude and present a different spatial pattern than the total changes in $P - E$ without using the C-C relation (Fig. 6a). This is understandable considering that the C-C relation is a thermodynamic equation and does not account for changes in circulations, while we have noticed from prior discussions that the dynamic component is the dominant contributor in the total changes of $P - E$. Worthy of mentioning here is that the C-C estimated total changes in $P - E$ portray predominantly positive changes across the TP (Fig. 7a), which is most likely due to rising temperature as the climate warms.

The above analysis based on ERA-Int demonstrates that changes in mean circulation controls changes in $P - E$. Contributions from transient eddy enhance the dynamic component over the southern and parts of the northern TP with complex terrain and large mountain chains. Over the central TP with relatively flat terrain, contributions from transient eddy offset the dynamic

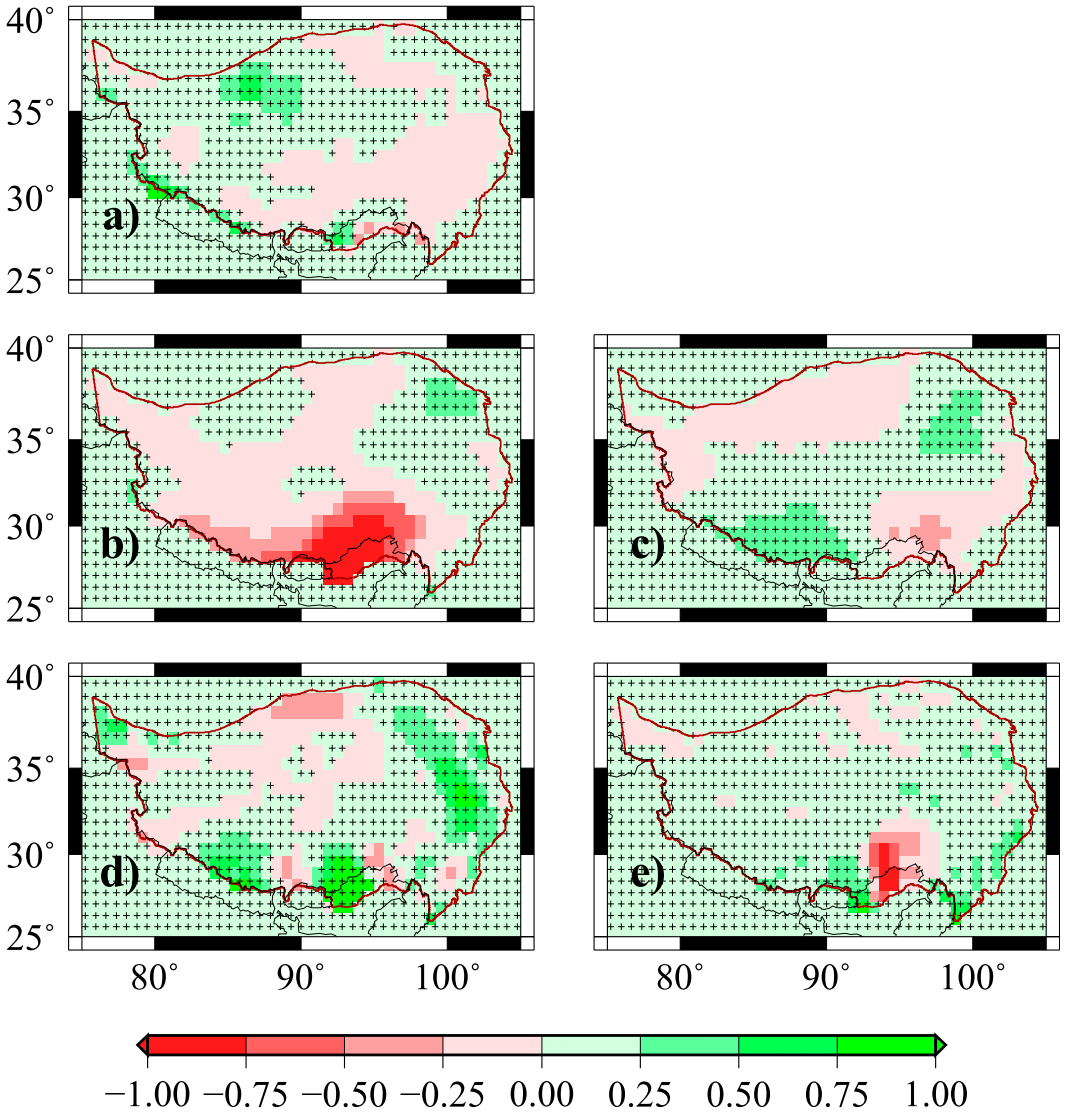

FIG. 5. Trends of (a) runoff (mm day^{-1} yr^{-1}) from the GLDAS ensemble mean, and $P - E$ estimates (mm day^{-1} yr^{-1}) from four global reanalyses [(b) NCEP-NCAR, (c) NCEP-DOE, (d) ERA-40, and (e) ERA-Int] over the TP for 1979–2011.

component, which results in small changes in $P - E$. Changes in mean humidity contribute positively to total changes in $P - E$ over the southern and central TP where low-tropospheric moisture flux could reach.

2) SEASONAL CYCLES OF $P - E$ CHANGES

Seasonal cycles of $P - E$ changes due to the three contributors averaged over the TP also show that MCD dominates over TH and TE during the wet season of May through September (Fig. 8) when large changes in $P - E$ or runoff occur. TH is generally small all year round, with positive changes only for June and negative changes only for March. Changes in transient eddy contribute positively to changes in $P - E$ in March–May and negatively in June–September. Monthly values (not shown) indicate that during the wet season the sum of MCD, TH, and TE accounts for approximately 100% of the changes in $P - E$ except for September for which the changes in $P - E$ and MCD, TH, and TE are about 5 to 8 times smaller than those in the other wet-season months. On average, the TP becomes wetter in the wet season and slightly drier or with little changes in the dry season in recent decades (Fig. 8). Because of the large magnitude of wetting in the wet season, the entire TP exhibits wetting trends at the annual time step (Table 2).

TABLE 3. Spatial correlation coefficients between changes in $P - E$, dynamic component MCD, thermodynamic component TH, transient eddy component TE, and changes in vertical wind field (ω) at 500 mb over the Tibetan Plateau. Statistically significant values at 99% (99.9%) confidence level based on the two-paired t test are denoted in boldface (marked with an asterisk). The degree of freedom for spatial correlation is 518.

	$P - E$ change	MCD	TH	TE
$P - E$ change	**1.0***	**0.88***	−0.12	−0.03
delta$(\omega)_{500\text{mb}}$	**−0.60***	**−0.65***	**0.13**	**0.23***

3) CAUSES OF MOISTURE CHANGES IN CONNECTION WITH GLOBAL WARMING

The above analyses demonstrate that while the TP gets wetter in general during the recent decades, spatial heterogeneity in moisture changes is evident as reflected by the drying trends in the southeastern TP and the wetting trends in the northwestern TP. As mentioned before, the C-C relation cannot be used to explain these spatial variations in moisture changes. It is tempting to assume that there may exist two kinds of competing forces such that one brings in the spatially uniform wetting changes while the other causes spatially varying changes in moisture over the TP. We propose that one force is related to global warming while the other force is related to changes in local circulations. Admittedly, changes in local circulations could also be related to global warming although it is nearly impossible to separate the local effects from the global effects given the feedbacks and nonlinear processes that are involved.

Possible connections with global warming can be investigated in terms of shifts in large-scale circulations, especially the Hadley circulation and the monsoon circulations, since they are two of the major circulations that transport heat and moisture from the tropics to the northern and southern midlatitudes. The Hadley circulation and the Asian monsoon circulations are intimately related to, among others, the East Asian jet stream and moisture transport that are important for the weather and climate over the TP. There has been mounting evidence from observations and climate model simulations that the Hadley circulation expands (e.g., Lu et al. 2007; Kang and Lu 2012; Tandon et al. 2013) and the summer monsoon circulations intensify (Wang et al. 2013; Sohn and Park 2010) under global warming.

The zonal and meridional wind components averaged across the longitudinal band of 90° to 98°E and their changes during the wet and warm season (May–September) and the dry and cold season (October–April) are examined in height–latitude cross sections (Fig. 9). This longitudinal band corresponds to where the meridional moisture flux passes through the TP. In the dry season, the East Asian westerly jet is strong with the center (i.e.,

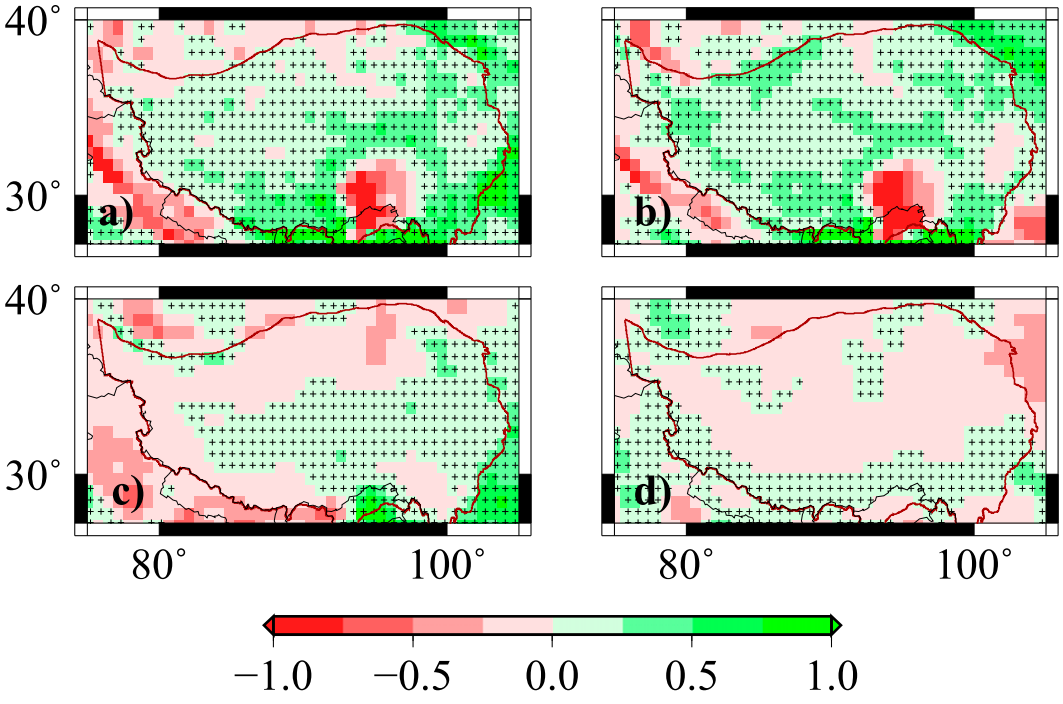

FIG. 6. (a) $P - E$ changes (mm day^{-1}) of 1998–2011 as compared to 1979–97 over the TP, and components of $P - E$ changes due to (b) changes in mean circulation (MCD), (c) changes in mean humidity (TH), and (d) transient eddies (TE) from ERA-Int.

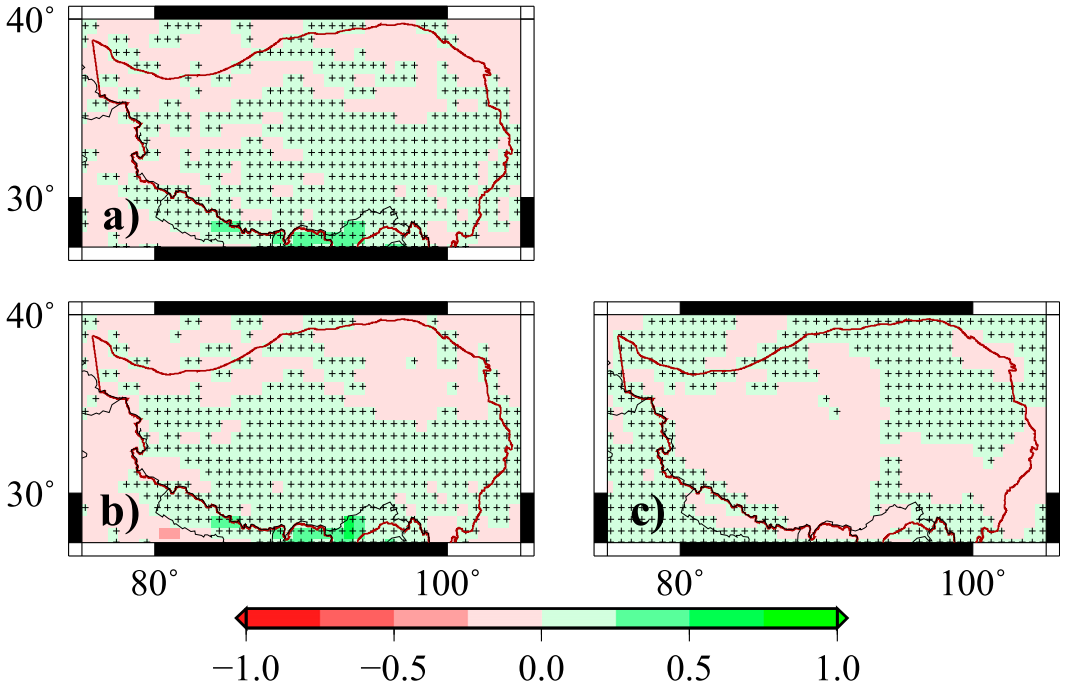

FIG. 7. (a) $P - E$ changes (mm day^{-1}) of 1998–2011 as compared to 1979–97 over the TP based on the Clausius–Clapeyron relation, and components of $P - E$ changes due to changes in (b) mean humidity and (c) transient eddies from ERA-Int.

jet streak) located at 150 mb and around 29°N just above the Himalaya Mountains for both 1998–2011 and 1979–97 (Fig. 9, panels a1 and a2). The northward and southward meridional flows meet around 30°N in the dry season, with cold and dry air prevailing in the north of the Himalaya Mountains throughout the vertical layer (Fig. 9, panels c1 and c2). The westerly jet is much weaker in the wet season than in the dry season and is also located farther north (around 40°N) (Fig. 9, panels b1 and b2). The meridional circulation during the wet season is characterized by southerly flow between the surface and 300 mb in the south of 40°N, which helps to transport moisture from the south to the north, and deep northerly flow in the north of 40°N (Fig. 9, panels d1 and d2).

Between 1979–97 and 1998–2011, the westerly jet shifts northward with the center displaced poleward by ~0.7° in both the dry and wet seasons (Fig. 9, panels a3 and b3). With this poleward shift of the westerly jet, the easterly trade winds (and the tropical moisture) may also expand poleward. This appears to be the case in the difference plots (Fig. 9, panels a3 and b3) where anomalous easterly flows prevail through a deep layer to the south of 40°N in both the dry and wet seasons. The anomalous easterly flow and to a lesser extent anomalous southerly flow at low levels over the TP in the wet season (Fig. 9, panels b3 and d3) contribute to the wet-season positive changes in $P - E$ (Fig. 8) as more air from the south and east or less air from the north and west corresponds to more moisture in this part of the world. The wet-season monsoon circulation to the south of the TP is also enhanced for 1998–2011 compared to 1979–97 (Fig. 9, panels d1–3) as manifested by the enhanced low-level southerly flow and upper-level northerly flow as well as the generally strengthened upward motion over the TP and the strengthened downward motion in the tropics (not shown), which helps to transport moisture from the south to the TP. On the other hand, anomalous westerly and northerly flows are identified over the TP (Fig. 9, panels a3 and c3), which may explain the dry-season negative changes in $P - E$ (Fig. 8). The findings here are also consistent with the changes in vertically integrated moisture flux over the

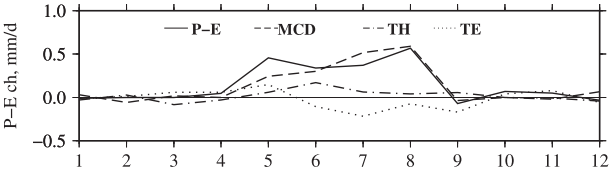

FIG. 8. Seasonal cycles of changes in $P - E$ (mm day^{-1}), mean circulation (MCD), mean humidity (TH), and transient eddies (TH) from ERA-Int in 1998–2011 relative to 1979–97 averaged over the TP. The x axis denotes the months.

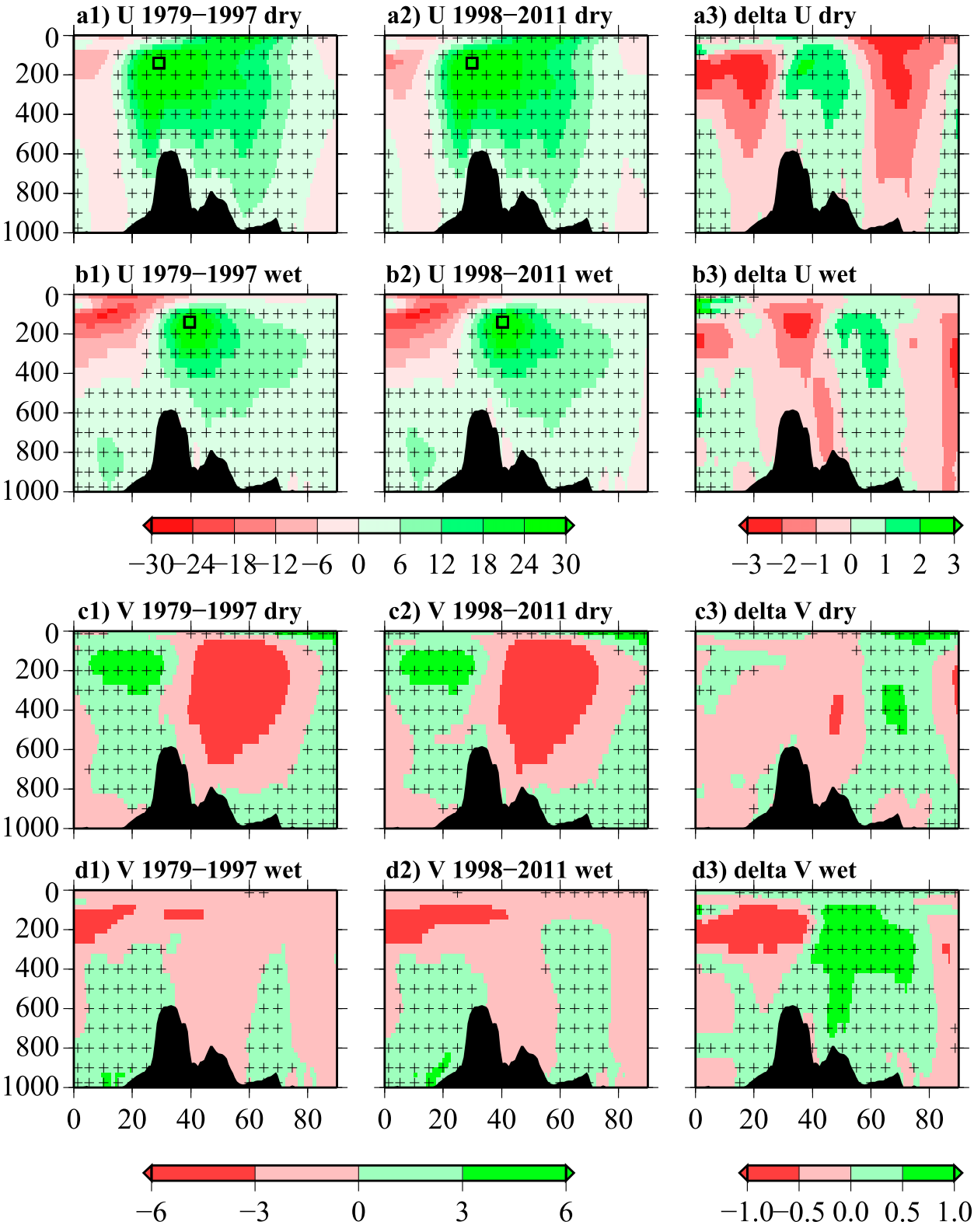

FIG. 9. Latitude–height cross sections featuring mean (a),(b) zonal (U) and (c),(d) meridional (V) wind components ($m\,s^{-1}$) in the (a),(c) dry and (b),(d) wet seasons of 1979–97 and 1998–2011 and changes (delta) in wind speed ($m\,s^{-1}$) in 1998–2011 relative to 1979–97 averaged over 90°–98°E from ERA-Int. Square marks the westerly jet streak location in (a) and (b). The x axis denotes latitude in °N and the y axis is pressure in millibars (1 mb = 1 hPa).

TP (not shown) where mainly positive changes are noted in the wet season while in the dry season negative changes are dominant.

Fu et al. (2006) documented the enhanced stratospheric cooling and tropospheric warming at midlatitude using satellite measurements. They noted that the jet streams and the tropical Hadley circulation shifted poleward by ~1° latitude in the summer and winter. Yin (2005) also reported a consistent poleward and upward shift and intensification of the storm tracks in AR4 climate model simulations. Based on these findings, researchers attribute the wetting at high latitudes to the poleward shift of moisture transport at lower troposphere since the Clausius–Clapeyron relation could not fully explain the hydrological cycle changes (Seager and Vecchi 2010; Seager et al. 2007, 2010; Sohn and Park 2010; Gao et al. 2011, 2012; Zhang et al. 2012). The subtropical jet streams represent the poleward bounds of the Hadley circulation. In this study, a poleward shift of ~0.7° latitude in the East Asian westerly jet and enhanced summer monsoon circulation are identified and the associated poleward transport of moisture can explain the general wetting trend over the TP on one hand, and on the other hand may provide the moisture needed for redistribution by local circulations as will be discussed below.

4) Causes of moisture changes in connection with the TP

The poleward shift of the jet stream and the intensification of the summer monsoon circulation and the related moisture transport tend to generate large-scale and spatially uniform changes in moisture. Changes in local circulations, however, could be responsible for redistributing and generating spatially varying changes in moisture over the TP. Here we will strive to demonstrate that changes in local circulations as represented by changes in vertical circulations are indeed responsible for the spatially varying changes in moisture over the TP in the wet season. We focus our discussions on the wet season because the changes in moisture over the TP are dominated by the changes in the wet season.

We first examine the changes in zonal and meridional wind components (u, v) at 200 and 500 mb (600 mb shows nearly identical patterns to 500 mb) in the wet season between 1979–97 and 1998–2011 and the results are presented in Figs. 10a–d. Anomalous easterly and northerly flows dominate over the TP at 200 mb except for the western tip of the TP where anomalous westerly and southerly flows are noted (Figs. 10a,b). At 500 mb (Figs. 10c,d), primarily anomalous easterly and southerly flows are identified over the TP. It is also clear that the changes in u and v components and the spatial gradients in both the latitudinal and longitudinal directions are generally larger at 200 mb than at 500 mb (Figs. 10a–d).

Changes in zonal and meridional wind components in turn result in spatially varying changes in divergence field at 200 and 600 mb as illustrated in Fig. 11. At 200 mb (Fig. 11a), anomalous divergence is dominant over the TP during the wet seasons. At 600 mb (Fig. 11b), anomalous convergence is noticed over the vast west TP during the wet season, with anomalous divergence and convergence scattered over the southeastern TP. Such changes in divergence correspond well to the changes in vertical wind field at 500 mb (Fig. 10e) as anomalous upward motion is generally located where either upper-level anomalous divergence or low-level anomalous convergence or both is found.

Recognizing that changes in $P - E$ over the TP occur predominantly in the wet season (Fig. 8), it becomes clear when comparing Fig. 5e with Fig. 10e that there exists close correspondence between the changes in vertical wind field and $P - E$ over the TP. For example, over the vast west TP, positive changes in $P - E$ correspond to anomalous upward motion while over the southeastern TP negative changes in $P - E$ correspond to anomalous downward motion. As a matter of fact, the spatial correlation between the changes in $P - E$ and vertical wind field at 500 mb shows statistically significant coefficient of -0.6 (negative because upward motion corresponds to negative vertical wind field in Pa s^{-1}) over the TP (Table 3). The spatial correlation between the dynamic component MCD and the changes in vertical wind field at 500 mb is even larger in magnitude at -0.65, which is also considerably higher in magnitude than the spatial correlation coefficients for the thermodynamic component TH (0.13) and transient eddy component TE (0.23) (Table 3). All these suggest that changes in local circulations as manifested by changes in divergence and vertical motion fields contribute in a significant way to the dynamic component MCD and is largely responsible for the spatially varying changes in $P - E$ over the TP.

To understand what might have caused the changes in divergence field, here we investigate the changes in zonal and meridional divergence components at 200 and 600 mb and the results are presented in Figs. 11c–f. At 600 mb (Figs. 11d,f), anomalous convergence is noted over the vast west TP for both components with anomalous divergence located mainly over southeastern and northeastern TP, the combination of which results in relatively strong anomalous convergence over the vast west TP and anomalous divergence over southeastern and northeastern TP at 600 mb in the wet season (Fig. 11b). At 200 mb (Figs. 11c,e), the zonal component corresponds to anomalous convergence over the TP except

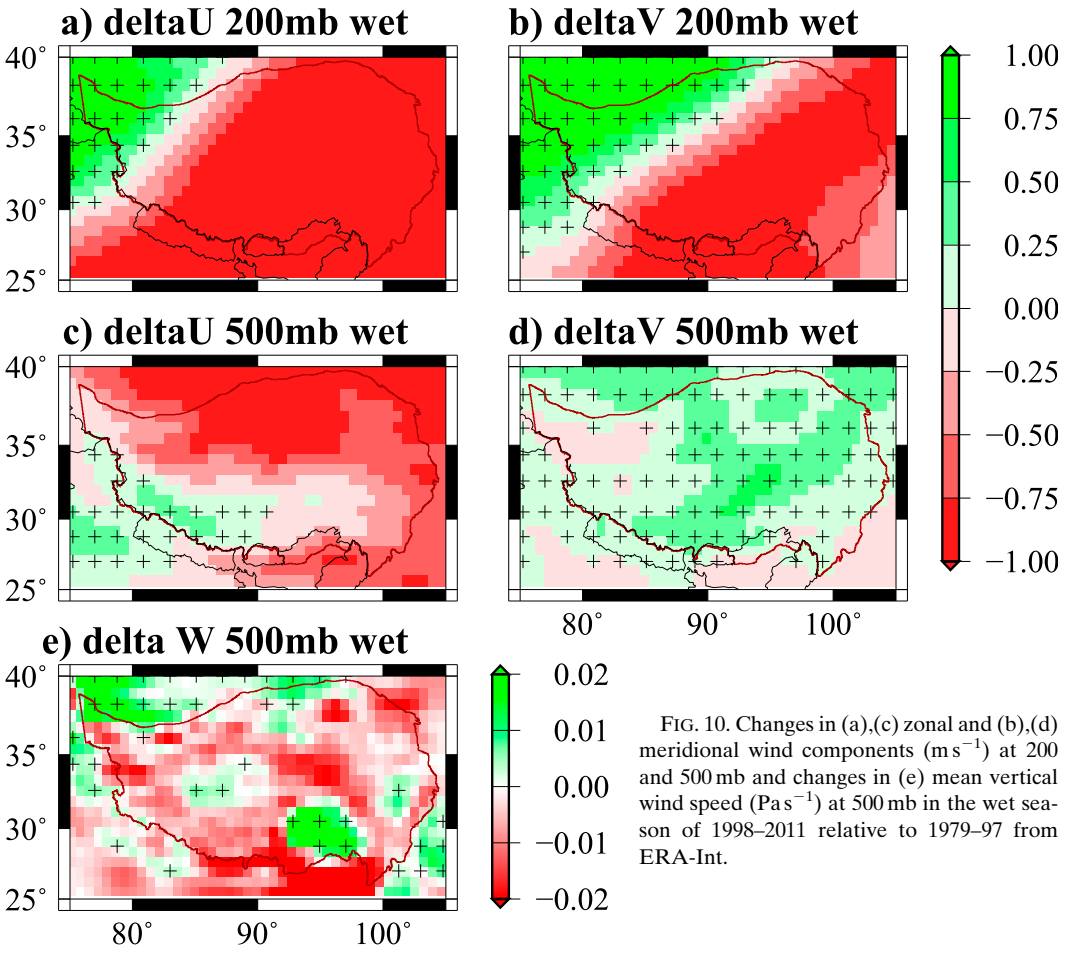

FIG. 10. Changes in (a),(c) zonal and (b),(d) meridional wind components ($m\,s^{-1}$) at 200 and 500 mb and changes in (e) mean vertical wind speed ($Pa\,s^{-1}$) at 500 mb in the wet season of 1998–2011 relative to 1979–97 from ERA-Int.

over the southeastern tip where anomalous divergence is identified (Fig. 11c), and the opposite is true for the meridional component (Fig. 11e). Because of the larger magnitude of the anomalous divergence than convergence, the total changes are dominated by anomalous divergence over the vast west TP at 200 mb in the wet season (Fig. 11a), which, together with the anomalous convergence at 600 mb, is responsible for the anomalous upward motion in the vast west TP (Fig. 10e). Similar arguments can also be applied to anomalous vertical motion elsewhere over the TP.

It is clear that owing largely to the anomalous divergence from the meridional component at 200 mb, anomalous upward motion is generated over the vast west TP, hence the wetting trends in the same region. The apparent question now is what has caused the changes in meridional wind component at 200 mb in the wet season as seen in Fig. 10b. Because of its location and extensive size, the TP exerts significant influence on regional and global climate through thermal and mechanical forcing (e.g., Manabe and Broccoli 1990; Yanai et al. 1992). Under global warming, the differential heating due to the TP and its surroundings could produce thermal winds that would affect the upper-level winds. To prove this, we examine the changes in zonal and meridional temperature gradients and the corresponding meridional and zonal thermal wind components at 200 mb following Holton (1992) in the wet season. Here temperature is the mean temperature between 700 and 200 mb. The results are shown in Fig. 12. Clearly, there are large changes in temperature gradients in the wet season (Fig. 12a), and the changes in zonal and meridional thermal wind components at 200 mb resemble those of zonal and meridional wind components at 200 mb with similar magnitude (cf. Figs. 12b and 10a, and Figs. 12c and 10b). Further proof is provided in Table 4 that shows spatial correlation coefficients between changes in zonal and meridional wind components at 200 mb and changes in meridional and zonal gradients of the mean temperature between 700 and 200 mb, respectively. All correlation coefficients are large and statistically significant (Table 4).

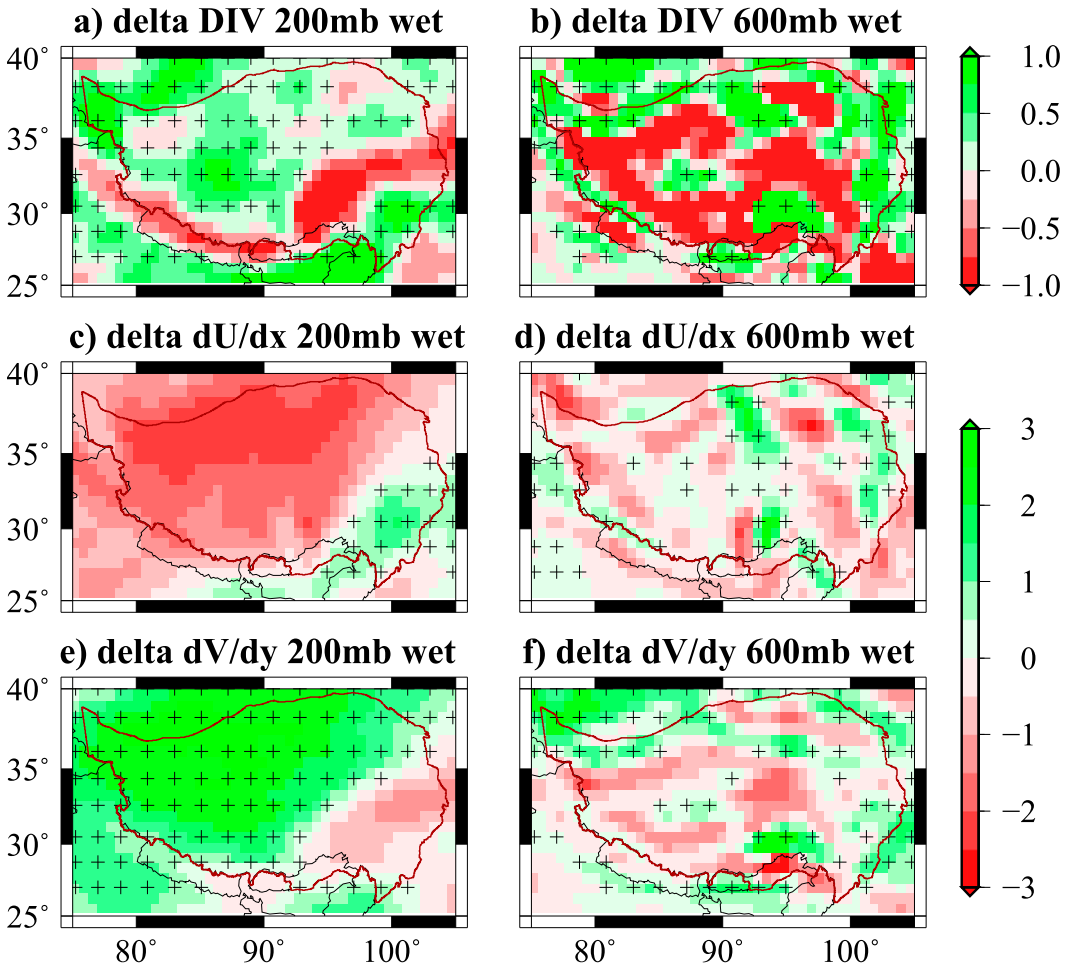

FIG. 11. Changes in (a),(b) total divergence and (c),(d) zonal and (e),(f) meridional divergence components ($10^{-6}\,s^{-1}$) at 200 and 600 mb, respectively, of 1998–2011 relative to 1979–97 in the wet season from ERA-Int.

4. Conclusions

Changes in moisture flux as represented by $P - E$ and the possible causes over the TP during 1979–2011 are examined based on the GLDAS ensemble mean runoff and reanalyses. ERA-Int is chosen due to the fact that it best resolves the spatial pattern of the GLDAS ensemble mean runoff climatology and temporal trends among the four widely used reanalysis datasets (NCEP–NCAR, NCEP–DOE, ERA-40, and ERA-Int), with the closest domain-averaged mean and the highest correlation.

The TP is getting wetter with large spatial variations. The climatologically humid southeastern TP becomes drier while the vast arid and semiarid northwestern TP is wetter. The C-C relation cannot be used to explain the changes in $P - E$ over the TP.

The analysis indicates that the dynamic component plays a key role over the TP in bringing about the changes in $P - E$ during the past decades. Changes in mean humidity contribute positively to changes in $P - E$ over southern and central TP where low-tropospheric moisture flux could reach. Contributions from transient eddy reinforce the dynamic component over southern and parts of the northern TP with complex terrain and large mountain chains. Over the central TP with relatively flat terrain, contributions from transient eddy offset the dynamic component and results in small changes in $P - E$.

Seasonally, the dynamic component contributes positively in a substantial way to changes in $P - E$ during the wet season of May through September. The thermodynamic and transient eddy components are much smaller all year round when compared to the dynamic component, with positive contributions for June (March–May) and negative contributions for March (June–September) for the thermodynamic (transient eddy) component.

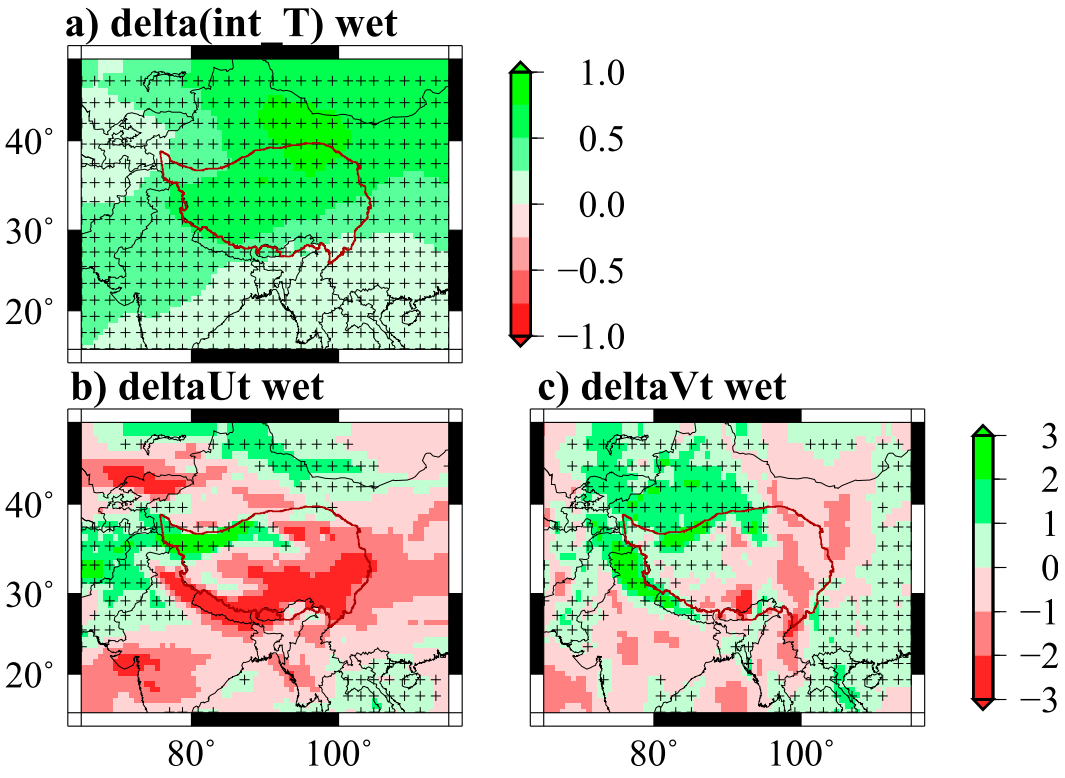

FIG. 12. Changes in (a) mean temperature between 700 and 200 mb (int_T, °C), (b) zonal thermal wind component (m s^{-1}), and (c) meridional thermal wind component (m s^{-1}) of 1998–2011 relative to 1979–97 for the wet season. Thermal wind components are computed using the mean temperature between 700 and 200 mb.

Through the examination of the zonal and meridional wind components and the vertically integrated moisture flux, we have noted the poleward shift of the East Asian westerly jet stream by 0.7° in both the dry and wet seasons as well as poleward moisture transport due to global warming. We argue that the poleward shift of the jet stream and moisture transport as well as the intensification of the summer monsoon circulation are responsible for the general wetting trend over the TP and possibly provide the moisture needed for redistribution by local circulations.

We further demonstrate that changes in local circulations in the wet season as manifested by changes in vertical motions are largely responsible for the spatially varying changes in moisture flux over the TP. The changes in vertical motions are accounted for by considering the changes in divergence field at upper and low levels, which are ultimately caused by changes in meridional wind component and to a lesser extent zonal wind component at upper levels through the thermal wind relationship due to the differential heating of the TP and its surroundings in the wet season.

The reanalysis datasets, especially ERA-Int in this case, are useful tools for diagnosing the changes in moisture and the possible cause both horizontally and vertically. However, caution has to be exerted in interpreting the ERA-Int-based analysis results since ERA-Int reveals deficiencies over the southeastern TP with large positive trends in moisture that are not supported by the GLDAS ensemble mean runoff. The deficiencies, which appear to be related to the overestimation of the contributions by changes in mean circulation over the area, should not affect the overall analysis and conclusions.

TABLE 4. Spatial correlation coefficients a) between changes in zonal wind component at 200 mb and changes in meridional gradient of the mean temperature between 700 and 200 mb and b) between changes in meridional wind component at 200 mb and changes in zonal gradient of the mean temperature between 700 and 200 mb for the wet season (WET) and annual mean (ANN) over the Tibetan Plateau. All values are statistically significant at a 99.9% confidence level based on the two-paired t test. The degree of freedom for spatial correlation is 518.

	WET	ANN
a)	0.69	0.72
b)	0.64	0.46

Acknowledgments. The reanalysis data used in this study are from the Research Data Archive (RDA) that is maintained by the Computational and Information Systems Laboratory (CISL) at the National Center for Atmospheric Research (NCAR). The GLDAS data are archived and distributed by the NASA's Goddard Earth Sciences (GES) Data and Information Services Center (DISC) and acquired through the Distributed Active Archive Center (DAAC). This work is jointly supported by National Basic Research Program of China (2013CB956004), National Natural Science Foundation of China (41322033), and "100-Talent" program granted by the Chinese Academy of Sciences to Yanhong Gao and Lan Cuo. We also thank the three anonymous reviewers for their thoughtful and constructive comments that greatly helped in improving the manuscript.

REFERENCES

Bao, X., and F. Zhang, 2013: Evaluation of NCEP–CFSR, NCEP–NCAR, ERA-Interim, and ERA-40 reanalysis datasets against independent sounding observations over the Tibetan Plateau. *J. Climate,* **26,** 206–214.

Bian, D., Z. Yang, L. Li, D. Chu, G. Zhuo, C. Bianba, Y. Zhaxi, and Y. Dong, 2006: The response of lake area change to climate variations in the North Tibetan Plateau during the last 30 years (in Chinese). *Acta Geogr. Sin.,* **61,** 510–518.

Chou, C., and C.-W. Lan, 2012: Changes in the annual range of precipitation under global warming. *J. Climate,* **25,** 222–235.

——, J. D. Neelin, C.-A. Chen, and J.-Y. Tu, 2009: Evaluating the "rich-get-richer" mechanism in tropical precipitation change under global warming. *J. Climate,* **22,** 1982–2005.

——, J. C. H. Chiang, C.-W. Lan, C.-H. Chung, Y.-C. Liao, and C.-J. Lee, 2013: Increase in the range between wet and dry season precipitation. *Nat. Geosci.,* **6,** 263–267, doi:10.1038/ngeo1744.

Conroy, J. L., and J. T. Overpeck, 2011: Regionalization of present-day precipitation in the greater monsoon region of Asia. *J. Climate,* **24,** 4073–4095.

Cuo, L., Y. Zhang, Q. Wang, L. Zhang, B. Zhou, Z. Hao, and F. Su, 2013: Climate change on the northern Tibetan Plateau during 1957–2009: Spatial patterns and possible mechanisms. *J. Climate,* **26,** 85–109.

Dee, D. P., and S. Uppala, 2009: Variational bias correction of satellite radiance data in the ERA-Interim reanalysis. *Quart. J. Roy. Meteor. Soc.,* **135,** 1830–1841.

——, and Coauthors, 2011: The ERA-Interim reanalysis: Configuration and performance of the data assimilation system. *Quart. J. Roy. Meteor. Soc.,* **137,** 553–597, doi:10.1002/qj.828.

Derber, J. C., D. F. Parrish, and S. J. Lord, 1991: The new global operational analysis system at the National Meteorological Center. *Wea. Forecasting,* **6,** 538–547.

Duan, A., and G. Wu, 2008: Weakening trend in the atmospheric heat source over the Tibetan Plateau during recent decades. Part I: Observations. *J. Climate,* **21,** 3149–3164.

——, and ——, 2009: Weakening trend in the atmospheric heat source over the Tibetan Plateau during recent decades. Part II: Connection with climate warming. *J. Climate,* **22,** 4197–4212.

Fu, Q., C. M. Johanson, J. M. Wallace, and T. Reichler, 2006: Enhanced mid-latitude tropospheric warming in satellite measurements. *Science,* **312,** 1179.

Gao, Y., J. Vano, C. Zhu, and D. P. Lettenmaier, 2011: Evaluating climate change over the Colorado River basin using regional climate models. *J. Geophys. Res.,* **116,** D13104, doi:10.1029/2010JD015278.

——, L. R. Leung, E. P. Salathé Jr., F. Dominguez, B. Nijssen, and D. P. Lettenmaier, 2012: Moisture flux convergence in regional and global climate models: Implications for droughts in the southwestern United States under climate change. *Geophys. Res. Lett.,* **39,** L09711, doi:10.1029/2012GL051560.

Ge, S., X. Tang, and H. Lu, 2008: Climatic characteristics of rainfall and rainy days during the last 35 years over the Qinghai-Xizang Plateau. *Acta Geogr. Sin.,* **63,** 924–930.

Guo, Q., Y. Yang, and X. Lu, 2011: Analysis of variation character of annual runoff in the Heihe River basin from 1957 to 2008 (in Chinese). *J. Water Res. Water Eng.,* **22,** 77–81.

Held, M. I., and B. J. Soden, 2006: Robust responses of the hydrological cycle to global warming. *J. Climate,* **19,** 5686–5699.

Holton, J. R., 1992: *An Introduction to Dynamic Meteorology*. Academic Press, 511 pp.

Huffman, G. J., R. F. Adler, E. F. Stocker, D. T. Bolvin, and E. J. Nelkin, 2003: Analysis of TRMM 3-hourly multi-satellite precipitation estimates computed in both real and post-real time. Preprints, *12th Conf. on Satellite Meteorology and Oceanography,* Long Beach, CA, Amer. Meteor. Soc., P4.11. [Available online at https://ams.confex.com/ams/pdfpapers/54906.pdf.]

Idso, S., 1981: A set of equations for full spectrum and 8- and 14-μm and 10.5- to 12.5-μm thermal radiation from cloudless skies. *Water Resour. Res.,* **17,** 295–304.

Kalnay, E., and Coauthors, 1996: The NCEP/NCAR 40-Year Reanalysis Project. *Bull. Amer. Meteor. Soc.,* **77,** 437–471.

Kanamitsu, M., W. Ebisuzaki, J. Woollen, S. Yang, J. J. Hnilo, M. Fiorino, and G. L. Potter, 2002: NCEP–DOE AMIP-II Reanalysis (R-2). *Bull. Amer. Meteor. Soc.,* **83,** 1631–1643.

Kang, S. C., Y. Xu, Q. You, W.-A. Flügel, N. Pepin, and T. Yao, 2010: Review of climate and cryospheric change in the Tibetan Plateau. *Environ. Res. Lett.,* **5,** 015101, doi:10.1088/1748-9326/5/1/015101.

Kang, S. M., and J. Lu, 2012: Expansion of the Hadley cell under global warming: Winter versus summer. *J. Climate,* **25,** 8387–8393.

Kassomenos, P. A., and G. R. McGregor, 2006: The interannual variability and trend of precipitable water over southern Greece. *J. Hydrometeor.,* **7,** 271–284.

Krause, P., S. Biskop, J. Helmschrot, W.-A. Flügel, S. Kang, and T. Gao, 2010: Hydrological system analysis and modelling of the Nam Co basin in Tibet. *Adv. Geosci.,* **27,** 29–36, doi:10.5194/adgeo-27-29-2010.

Li, R., S. Lu, B. Han, and Y. Gao, 2012: Preliminary comparison and analyses of air temperature at 2-m height between three reanalysis datasets and observation in the east of Qinghai-Xizang Plateau (in Chinese). *Plateau Meteor.,* **31,** 1488–1502.

Liu, X., and B. Chen, 2000: Climatic warming in the Tibetan Plateau during recent decades. *Int. J. Climatol.,* **20,** 1729–1742.

Lorenz, D. J., and E. T. DeWeaver, 2007: The response of the extratropical hydrological cycle to global warming. *J. Climate,* **20,** 3470–3484.

Lu, J., G. A. Vecchi, and T. Reichler, 2007: Expansion of the Hadley cell under global warming. *Geophys. Res. Lett.,* **34,** L06805, doi:10.1029/2006GL028443.

Manabe, S., and A. J. Broccoli, 1990: Mountains and arid climate of middle latitudes. *Science,* **247,** 192–195.

Moore, G. W. K., 2012: Surface pressure record of Tibetan Plateau warming since the 1870s. *Quart. J. Roy. Meteor. Soc.,* **138,** 1999–2008.

Pan, B., and J. Li, 1996: Qinghai-Tibetan Plateau: A driver and amplifier of the global climatic change. *J. Lanzhou Univ.,* **32,** 108–115.

Rodell, M., and Coauthors, 2004: The Global Land Data Assimilation System. *Bull. Amer. Meteor. Soc.,* **85,** 381–394.

Schiemann, R., D. Lüthi, and C. Schär, 2008: Seasonality and interannual variability of the westerly jet in the Tibetan Plateau region. *J. Climate,* **22,** 2940–2957.

Seager, R., and G. A. Vecchi, 2010: Greenhouse warming and the 21st century hydroclimate of southwestern North America. *Proc. Natl. Acad. Sci. USA,* **107,** 21 277–21 282, doi:10.1073/pnas.0910856107.

——, and N. Naik, 2012: A mechanism-based approach to detecting recent anthropogenic hydroclimate change. *J. Climate,* **25,** 236–261.

——, and Coauthors, 2007: Model projections of an imminent transition to a more arid climate in southwestern North America. *Science,* **316,** 1181–1184, doi:10.1126/science.1139601.

——, N. Naik, and G. A. Vecchi, 2010: Thermodynamic and dynamic mechanisms for large-scale changes in the hydrological cycle in response to global warming. *J. Climate,* **23,** 4651–4668.

Shapiro, R., 1987: A simple model for the calculation of the flux of direct and diffuse solar radiation through the atmosphere. Air Force Geophysics Laboratory Tech. Rep. AFGL-TR-87-0200, 40 pp.

Shi, Y., Y. Shen, E. Kang, D. Li, Y. Ding, G. Zhang, and R. Hu, 2007: Recent and future climate change in northwest China. *Climatic Change,* **80,** 379–393.

Simmons, A., S. Uppala, D. Dee, and S. Kobayashi, 2006: ERA-Interim: New ECMWF reanalysis products from 1989 onwards. *ECMWF Newsletter,* No. 110, ECMWF, Reading, United Kingdom, 25–35.

Sohn, B. J., and S.-C. Park, 2010: Strengthened tropical circulations in past three decades inferred from water vapor transport. *J. Geophys. Res.,* **115,** D15112, doi:10.1029/2009JD013713.

Solomon, S., D. Qin, M. Manning, Z. Chen, M. Marquis, K. Averyt, M. M. B. Tignor, and H. L. Miller Jr., 2007: *Climate Change 2007: The Physical Science Basis.* Cambridge University Press, 996 pp.

Tandon, N. F., E. P. Gerber, A. H. Sobel, and L. M. Polvani, 2013: Understanding Hadley cell expansion versus contraction: Insights from simplified models and implications for recent observations. *J. Climate,* **26,** 4304–4321.

Tian, L., T. Yao, K. MacClune, J. W. C. White, A. Schilla, B. Vaughn, R. Vachon, and K. Ichiyanagi, 2007: Stable isotopic variations in west China: A consideration of moisture sources. *J. Geophys. Res.,* **112,** D10112, doi:10.1029/2006JD007718.

Trenberth, K. E., and C. J. Guillemot, 1995: Evaluation of the global atmospheric moisture budget as seen from analyses. *J. Climate,* **8,** 2255–2272.

Turk, F. J., G. Rohaly, J. D. Hawkins, E. A. Smith, A. Grose, F. S. Marzano, A. Mugnai, and V. Levizzani, 2000: Analysis and assimilation of rainfall from blended SSM/I, TRMM, and geostationary satellite data. Preprints, *10th Conf. on Satellite Meteorology and Oceanography,* Long Beach, CA, Amer. Meteor. Soc., 66–69.

Uppala, S. M., and Coauthors, 2005: The ERA-40 Re-Analysis. *Quart. J. Roy. Meteor. Soc.,* **131,** 2961–3012, doi:10.1256/qj.04.176.

Wang, A., and X. Zeng, 2012: Evaluation of multi-reanalysis products with in situ observations over the Tibetan Plateau. *J. Geophys. Res.,* **117,** D05102, doi:10.1029/2011JD016553.

Wang, B., J. Liu, H. Kime, P. J. Webster, S. Yim, and B. Xiang, 2013: Northern Hemisphere summer monsoon intensified by mega-El Niño/Southern Oscillation and Atlantic multidecadal oscillation. *Proc. Natl. Acad. Sci. USA,* **110,** 5347–5352.

Wentz, F. J., L. Ricciardulli, K. Hilburn, and C. Mears, 2007: How much more rain will global warming bring? *Science,* **317,** 233–235, doi:10.1126/science.1140746.

Wu, S., Y. Yin, D. Zheng, and Q. Yang, 2007: Climatic trends over the Tibetan Plateau during 1971–2000. *J. Geogr. Sci.,* **17,** 141–151, doi:10.1007/s11442-007-0141-7.

Wu, Y., and L. Zhu, 2008: The response of lake-glacier variations to climate change in Nam Co Catchment, central Tibetan Plateau, during 1970–2000. *J. Geogr. Sci.,* **18,** 177–189, doi:10.1007/s11442-008-0177-3.

Yanai, M., C. Li, and Z. Song, 1992: Seasonal heating of the Tibetan Plateau and its effects on the evolution of the Asian summer monsoon. *J. Meteor. Soc. Japan,* **70,** 319–351.

Yang, K., B. Ye, D. Zhou, B. Wu, T. Foken, J. Qin, and Z. Zhou, 2011: Response of hydrological cycle to recent climate changes in the Tibetan Plateau. *Climatic Change,* **109,** 517–534, doi:10.1007/s10584-011-0099-4.

Yao, T. L., and Coauthors, 2012: Different glacier status with atmospheric circulations in Tibetan Plateau and surroundings. *Nat. Climate Change,* **2,** 663–667, doi:10.1038/nclimate1580.

Yin, J. H., 2005: A consistent polarward shift of the storm tracks in simulations of 21st century climate. *Geophys. Res. Lett.,* **32,** L18701, doi:10.1029/2005GL023684.

Yin, Y., S. Wu, D. Zhao, D. Zheng, and T. Pan, 2012: Impact of climate change on actual evapotranspiration on the Tibetan Plateau during 1981–2010 (in Chinese). *Acta Geogr. Sin.,* **67,** 1471–1481.

You, Q., S. Kang, E. Aguilar, and Y. Yan, 2008: Changes in daily climate extremes in the eastern and central Tibetan Plateau during 1961–2005. *J. Geophys. Res.,* **113,** D07101, doi:10.1029/2007JD009389.

Zhang, X., J. He, J. Zhang, I. Polyakov, R. Gerdes, J. Inoue, and P. Wu, 2012: Enhanced polarward moisture transport and amplified northern high-latitude wetting trend. *Nat. Climate Change,* **3,** 47–51, doi:10.1038/nclimate1631.

Zhu, L., M. Xie, and Y. Wu, 2010: Quantitative analysis of land area variations and the influence factors from 1971 to 2004 in the Nam Co basin of the Southern Tibet Plateau. *Chin. Sci. Bull.,* **55,** 1294–1303, doi:10.1007/s11434-010-0015-8.